The Cold Front of 15 April 1994 over the Central United States. Part I: Observations

B. B. DEMOZ,* D. O'C. STARR,* K. D. EVANS,+ A. R. LARE,# D. N. WHITEMAN,* G. SCHWEMMER,* R. A. FERRARE,@ J. E. M. GOLDSMITH,& AND S. E. BISSON&

*NASA Goddard Space Flight Center, Greenbelt, Maryland
+University of Maryland, Baltimore County, Baltimore, Maryland
#L-3 Communications Government Services, Inc., Chantilly, Virginia
@NASA Langley Research Center, Hampton, Virginia
&Sandia National Laboratory, Livermore, California

(Manuscript received 24 February 2004, in final form 19 October 2004)

ABSTRACT

Detailed observations of the interactions of a cold front and a dryline over the central United States that led to dramatic undulations in the boundary layer, including an undular bore, are investigated using high-resolution water vapor mixing ratio profiles measured by Raman lidars. The lidar-derived water vapor mixing ratio profiles revealed the complex interaction between a dryline and a cold-frontal system. An elevated, well-mixed, and deep midtropospheric layer, as well as a sharp transition (between 5- and 6-km altitude) to a drier region aloft, was observed. The moisture oscillations due to the undular bore and the mixing of the prefrontal air mass with the cold air at the frontal surface are all well depicted. The enhanced precipitable water vapor and roll clouds, the undulations associated with the bore, the strong vertical circulation and mixing that led to the increase in the depth of the low-level moist layer, and the subsequent lifting of this moist layer by the cold-frontal surface, as well as the feeder flow behind the cold front, are clearly indicated.

A synthesis of the Raman lidar–measured water vapor mixing ratio profiles, satellite, radiometer, tower, and Oklahoma Mesonet data indicated that the undular bore was triggered by the approaching cold front and propagated south-southeastward. The observed and calculated bore speeds were in reasonable agreement. Wave-ducting analysis showed that favorable wave-trapping mechanisms existed; a low-level stable layer capped by an inversion, a well-mixed midtropospheric layer, and wind curvature from a low-level jet were found.

1. Introduction

During evenings and early morning hours, the lower atmosphere commonly acts as a waveguide for the propagation of a variety of atmospheric waves that occur in a wide range of both temporal and spatial scales. The undular bore, a propagating disturbance characterized by an abrupt increase in ground-level pressure associated with an increase in ground-level temperature and a shift in wind direction often consisting of wavelike oscillations, is one example that uses the stably stratified layer within the lower atmosphere as a waveguide. Observations of bores have been reported by several authors including Clarke et al. (1981), Shreffler and Binkowski (1981), Smith et al. (1982), Doviak and Ge (1984), Haase and Smith (1984), Simpson (1987), Cheung and Little (1990), Fulton et al. (1990), Koch et al. (1991), Locatelli et al. (1998), Koch and Clark (1999), and others. The Morning Glory, a frequent phenomenon near the Gulf of Carpentaria in northern Australia, reported extensively by Clarke et al. (1981), is an undular bore propagating along a temperature inversion generated by the interaction of a sea-breeze front with a nocturnal maritime inversion.

Several theories have been proposed as possible generation mechanisms for atmospheric bores. Numerical computations of density currents encountering strong stratification near the ground (Crook and Miller 1985; Crook 1986, 1988; Noonan and Smith 1986; Haase and Smith 1989), cool air behind colliding gravity currents (Clarke 1983; Noonan and Smith 1986; Wakimoto and Kingsmill 1995), thunderstorm outflows (Shreffler and Binkowski 1981; Doviak et al. 1989; Fulton et al. 1990), and mesoscale fronts (Smith et al. 1982; Koch et al.

Corresponding author address: Belay B. Demoz, NASA GSFC, Code 912, Greenbelt, MD 20771.
E-mail: belay.b.demoz@nasa.gov

© 2005 American Meteorological Society

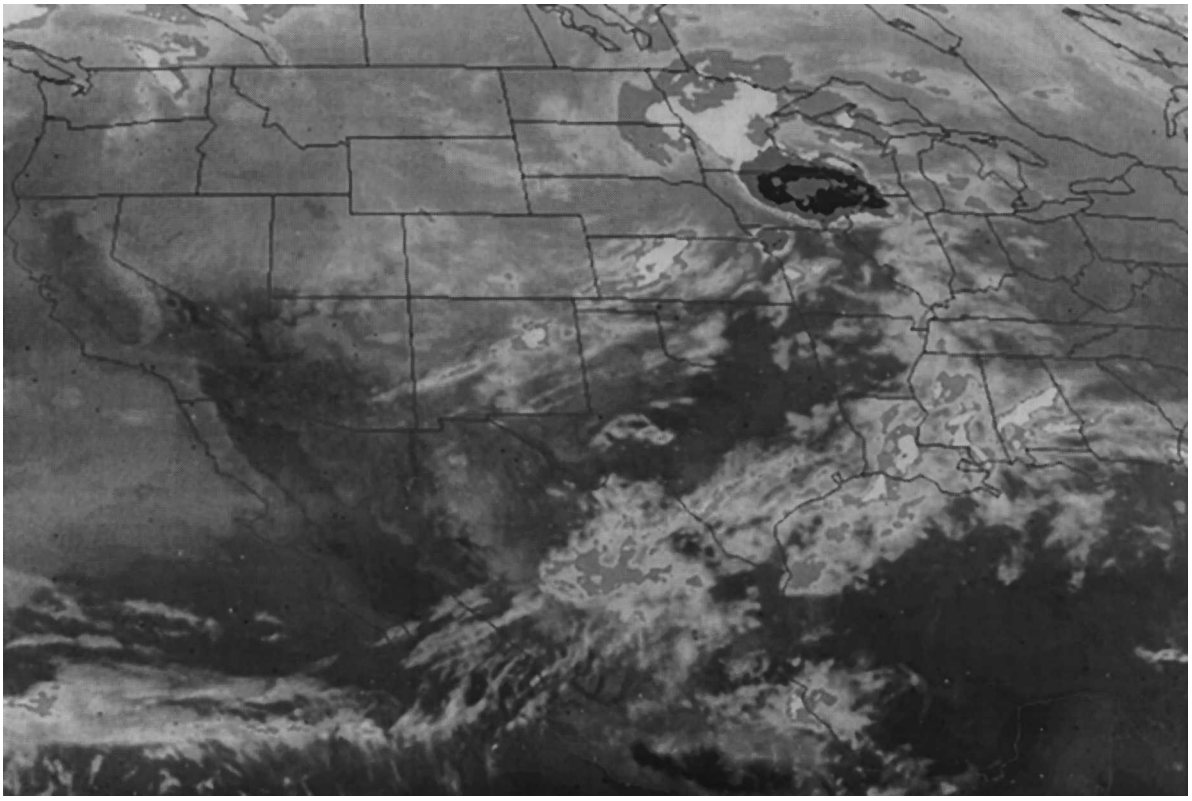

FIG. 1. Geostationary Operational Environmental Satellite (GOES) enhanced infrared imagery at 0400 UTC 15 Apr 1994.

1991; Koch and Clark 1999) interacting with an existing stable layer may trigger bore wave phenomenon. Laboratory simulations of gravity-current-induced atmospheric bores have also been reported (Maxworthy 1980; Rottman and Simpson 1989). A recent discussion of gravity currents and bore waves can be found in Koch and Clark (1999).

In this study, we present an analysis of Raman lidar–sensed profiles of water vapor mixing ratio and supporting surface mesonet, satellite imagery, rawinsonde, tower, and microwave-radiometer-measured precipitable water vapor data, which show distinct undular bore and other wave activity associated with a cold-frontal passage and dryline conditions. The data for this study were recorded on the night of 14–15 April 1994 (all times hereafter are UTC) during the Atmospheric Radiation Measurement (ARM) Remote Cloud Sensing (RCS) intensive operations period (IOP) at the Southern Great Plains Climate and Radiation Testbed (CART) near Lamont, Oklahoma (Stokes and Schwartz 1994; Ackerman and Stokes 2003). The purpose of this work is to demonstrate the utility of Raman lidar systems for measuring the vertical and temporal evolutions of atmospheric stratification (via water vapor mixing ratio) leading to undular bore activity during a *dryline–frontal merger* (Shapiro et al. 1985; Parsons et al. 2000). In addition, it is the only lidar-based observational study that clearly illustrates the time–height evolution of the interaction between a dryline, undular bore, and a cold front. This paper focuses only on the observations; numerical simulations and wavelet-based-analysis aspects of the data will follow in a subsequent work.

Section 2 describes the synoptic conditions, time series surface mesonet observations, and sounding ascent datasets. Raman lidar and microwave radiometer measurements are presented in section 3. Theoretical considerations are discussed in section 4, and a summary and conclusions are given in section 5.

2. Meteorological data

a. Synoptic conditions

Satellite and surface charts showed a low pressure system that moved south-southeast into northern Texas and Oklahoma early on 15 April 1994 (Fig. 1). At the same time, much of eastern Oklahoma and Texas were under the influence of a northward-moving air mass of high moisture content from the Gulf of Mexico while the western parts were influenced by a dry air mass from the Mexican Plateau. This resulted in a line of strong dewpoint temperature and wind direction gradi-

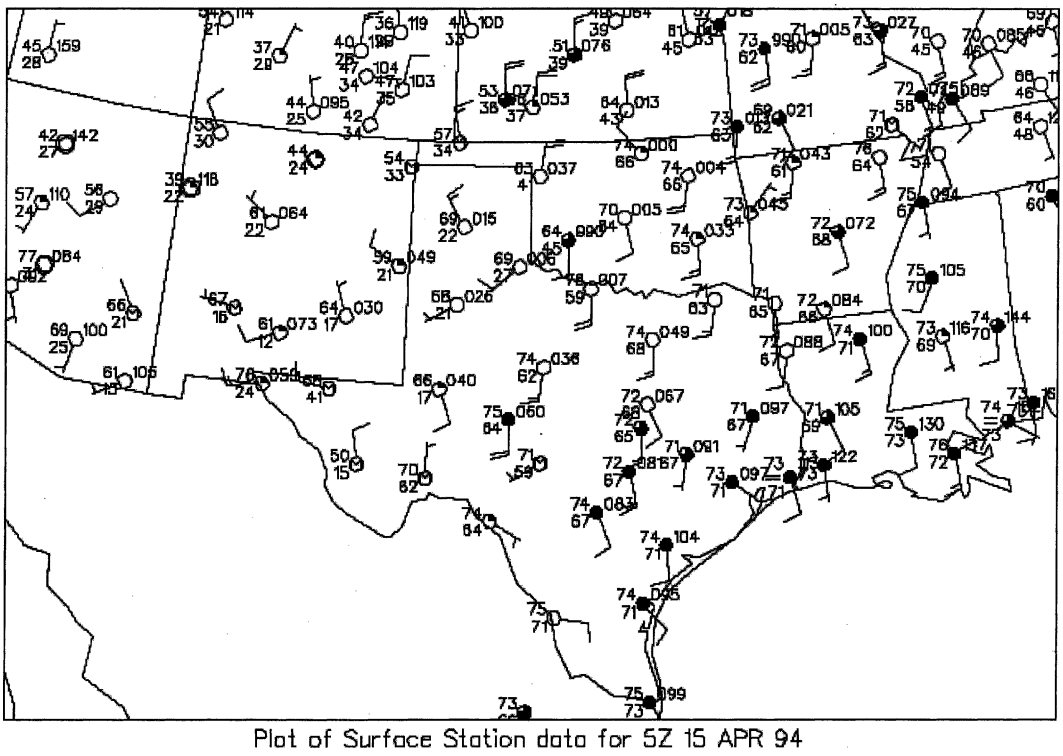

FIG. 2. Surface observations made at National Weather Service (NWS) stations at 0500 UTC 15 Apr 1994 showing winds, temperature (atmospheric and dewpoint), and sky conditions.

ent that traversed Oklahoma and Texas from southwest to northeast. Temperatures recorded at stations west of this line, in the dry air, were typically cooler than those recorded at stations east of the line (Fig. 2).

Streamline and dewpoint temperature analysis of data recorded by the Oklahoma Mesonet stations also showed a sharp moisture gradient traversing the state roughly north–south (Fig. 3). A sequence of streamline analysis plots (not shown here) revealed that a zone of sharp moisture gradient moved westward early during the night but later slowed and eventually reversed in direction as the cold front approached, indicated by the wind and streamline shifts. This movement of the moist air mass was consistent with the general behavior of dryline conditions and movements that are common to the region during late spring and early summer (Peterson 1983; Schaefer 1986). In summary, the convergence of the moist air mass from the Gulf, the dry air from the Mexican Plateau, and a cold-frontal system near the experiment site led to intense wave activity (including an undular bore) over the CART site.

b. Surface observations at CART

Observations of wind, temperature, pressure, and tower mixing ratio on 14–15 April 1994 at the CART site are plotted in Fig. 4. The wind direction between 0000 and 0430, prior to the undular bore, was mainly from the southwest except for a brief oscillation at about 0100 and a series of oscillations around 0320 (Figs. 4a, 4e, and 4f). The 0320 oscillations coincided with the arrival of the abrupt moisture increase and the location of the dryline. Between 0430 and 0500, wind speed and direction were highly oscillatory. Wind speeds from as high as about 12 $m\,s^{-1}$ to as low as 2 $m\,s^{-1}$ were recorded. Starting about 0500, the winds veered and increased in strength.

The pressure (temperature) data at CART were consistently increasing (decreasing) after about 0430, indicating the approach and then passage of the cold front (Figs. 4c, 4h and 4b, 4g). Embedded in the pressure trend, a series of impulse pressure increases (steps) similar in manner to those described by Tepper (1950) were observed. The largest of these pressure jumps, a rise of about 1.9 mb in less than 2 min, occurred at 0430 followed by a series of small-amplitude oscillations. This pressure jump, associated with roll clouds (visually observed), the shift in winds, and temperature increase, was identified as an atmospheric undular bore (Stull 1988). Two distinct peaks in wind direction change were observed. The first occurred at 0435 and was associated with wind veering from 260° to 305° (direction of the bore movement) and then back to 260°. This was

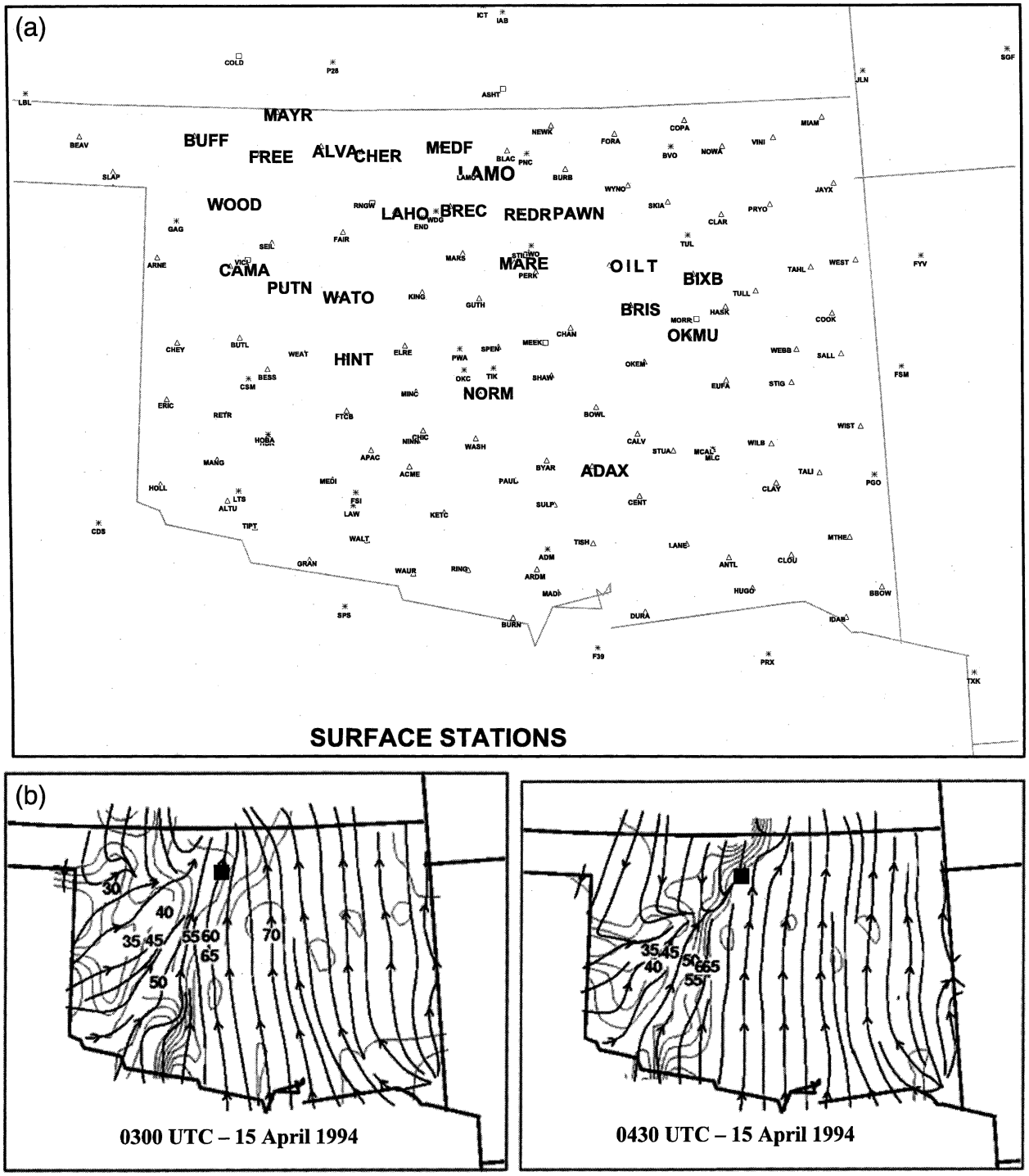

FIG. 3. (a) Map showing the Oklahoma Mesonet surface stations (see http://www.mesonet.org/overview for details of all stations) and the location of the DOE ARM CART station (LAMO) where the RCS IOP instrumentation was located. Stations used in Figs. 5–7 are highlighted. The two lines shown are about 300 km each. (b) Streamline and dewpoint temperature (°F) analysis of the Oklahoma Mesonet station data at 0300 and 0430 UTC 15 Apr 1994. The CART site, in north-central Oklahoma, is indicated by a square box.

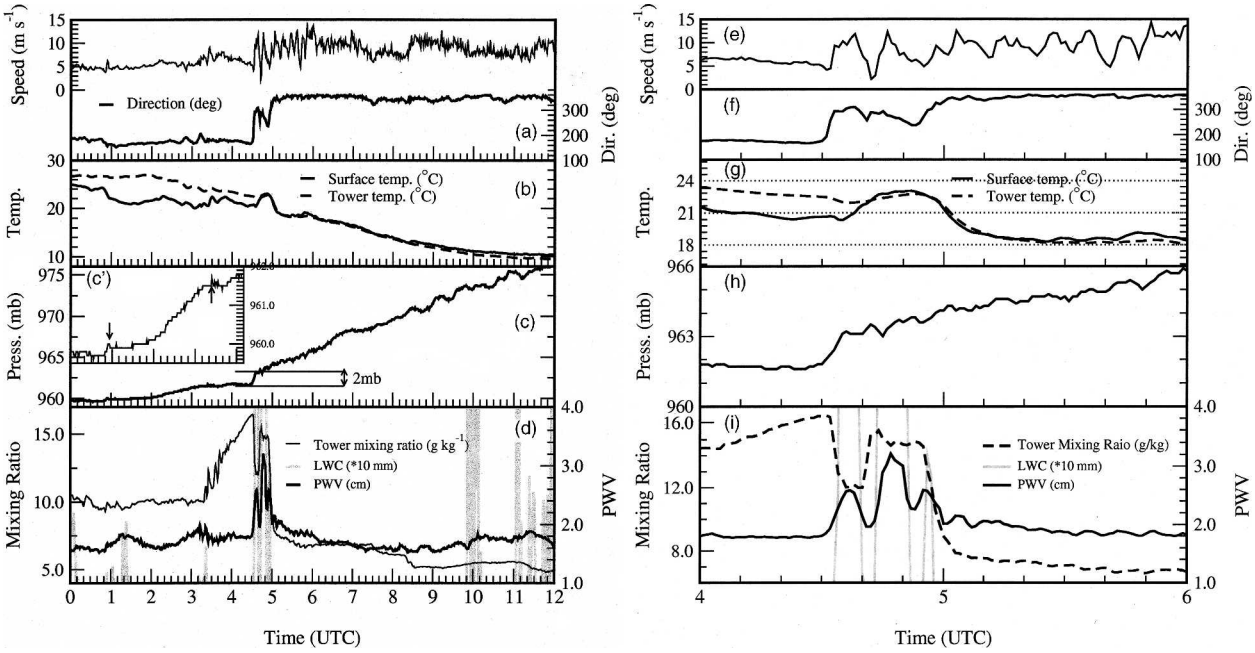

FIG. 4. Surface observations at the ARM CART site near Lamont, OK, on 15 Apr 1994. Plotted vs time are (a), (e), and (f) wind speed (m s^{-1}) and direction (°), (b), (g) temperature (°C) as measured on the surface and 60 m above ground using the instrumented tower, (c), (h) surface pressure (mb) (a magnified plot of the pressure records between 0000 and 0400 UTC is also shown in c′), and (d), (i) microwave-radiometer-measured precipitable water vapor (cm) and water vapor mixing ratio (g kg^{-1}) from an instrumented tower. Microwave-radiometer-measured integrated liquid water (multiplied by a factor of 10; in mm) is used to indicate "cloud" occurrence. Note that (e)–(i) are expanded plots of the variables between 0400 and 0600 UTC.

followed by a second hump to almost 300° and back to 230° before becoming constant at about 340° once the cold-frontal air mass dominated. Wind speed peaks also coincided well with wind direction and were about 11–12 m s^{-1} between 0430 and 0450. The temperature at the surface and tower during the bore was dominated by a temperature increase (one of the main characteristics of a bore) associated with the downward mixing of air from above the inversion level (discussed below). A temperature perturbation of about 3°C coincided with observation of the largest change in wind speed and direction.

Prior to 0430, a series of small-amplitude pressure jumps (0.3 to 0.4 mb) were recorded. The pressure jumps around 0100 and 0320 were most notable and were associated with wind speed and direction oscillations and temperature perturbations (a faint dip followed by a pronounced peak). Temperature perturbations of about 0.5°C were observed at 0100 with a slightly larger one around 0320, which was followed by another hump near 0350. The pressure jump recorded around 0320 was also immediately followed by small-scale oscillations similar to what would be expected by weak bore-induced oscillations.

Numerous, less pronounced, pressure jumps were also recorded during the earlier part of the day; however, their effect on wind and temperature perturbations were not appreciable. In addition, the surface temperature record also showed two relatively large depressions, between about 0100 and 0220 and between 0220 and 0330, which corresponded in time with remnants of midlevel cirrus clouds that were in the region earlier in the daytime. In this analysis, we will mainly focus on the 0100, 0320, and 0430 perturbations.

Combined with temperature, wind, and pressure data, the mixing ratio records reveal an interesting picture of the lower atmosphere during the dryline and bore periods. Measurements of water vapor mixing ratio made by the tower (60 m high) instrument at the time are presented in Figs. 4d and 4i. The mixing ratios were nearly constant at about 9.5 g kg^{-1} prior to 0320, except for small-amplitude oscillations (coincident with pressure and temperature bumps) near 0100. Between 0320 and 0430, when the dryline was just west of the station, a sharp oscillatory rise in mixing ratio values was recorded. This was associated with the borelike pressure jump and temperature increase, as well as wind speed and direction changes.

Between 0430 and 0500, during the undular bore, the mixing ratio profile of the lower atmosphere was dominated by vigorous bore undulations. During the first wave peak, mixing ratio values dropped from 16 to 12 g

kg^{-1}, and the peak was marked by a brief decrease in surface and tower temperatures (~1°C). This drop in temperature and moisture is attributed to the adiabatic ascent of air parcels during the formation of the first cloud band. The subsequent rise in mixing ratio to about 15.5 g kg^{-1} during the second and third cloud bands is also recorded. Note that there was almost no drop in mixing ratio separating the latter two wave peaks. A possible explanation may be that the mixing was not as vigorous so the air parcels did not mix down to instrument levels to be recorded, which could also explain the lack of temperature perturbations. Precipitable water vapor (PWV; cm) and integrated liquid water (LWV; mm) as measured by a microwave radiometer (Liljegren and Lesht 1996) are also plotted in Fig. 4, indicating the undulations associated with the 0100, 0320, and 0430 pressure jumps and location of clouds.

Finally, a combination of the surface and tower wind, moisture, and temperature data locate the passage to be close to 0500. However, proximity of the bore to the onset of the surface cold front led to superposition of the bore-front signatures, which blurred determination of the exact time of surface cold-frontal passage and its vertical characteristics at the site. The leading edge of the cold front had a complicated structure as will be shown later, using the Raman lidar observations of low-level moisture profile data.

c. *Surface observations at selected mesonet stations*

Five-minute averaged time series plots of pressure, temperature, and wind vector at selected mesonet stations roughly aligned along a northwest–southeast line in northern Oklahoma (Fig. 3) are shown in Figs. 5 and 6. A number of gravity waves (e.g., mesonet station BREC at 0230) and/or other perturbations are present in the data. However, this analysis is restricted to the undular bore as manifested by appreciable wind (Fig. 6), temperature, and pressure perturbations at the selected stations.

In Fig. 6, the bore can be easily identified as a disturbance traveling from northwest to southeast, across the northern part of the state. The bore arrived at stations near the CART Central Facility (LAHO, BREC, and REDR) between 0430 and 0530. The associated shifts in speed and direction were similar to those observed at CART. The pressure jumps at LAHO, BREC, and REDR were close to 2.2, 1.6, and 2.3 mb and were accompanied by temperature increases of 2°, 2.8°, and slightly less than 1°C, respectively (Fig. 5). At LAHO, and to a lesser extent at REDR, weak borelike signatures similar to those observed at CART were also present in the temperature and pressure data prior to the arrival of the undular bore. A pressure jump observed ahead of the bore over BREC at about 0300 was associated with a decrease in temperature and a very brief wind shift (Fig. 6). To date, we have not resolved this signature (seen only at BREC).

At stations northwest of CART (BUFF, MAYR, and WOOD), the bore/front signatures are less distinct. At BUFF, and to some extent at MAYR, an abrupt decrease in temperature together with a relatively gradual increase in pressure is more indicative of a cold front than a bore. At WOOD, however, a sharper increase in pressure (~0320) is more representative of a borelike phenomenon. At about 0320, just before the cold-frontal air mass began to dominate (Fig. 6), the temperature increased by about 1°C, associated with a steep rise in pressure and accompanied by an abrupt but brief change in wind speed and direction. The pressure jump at WOOD, and stations in the northwest corner, is not as distinct as what was recorded at stations near CART. One reason for the absence and/or faint bore signatures over these northwest stations may be that the low-level moist air from the Gulf, which was acting as a duct over CART (and stations east), did not reach as far into the northwest corner of Oklahoma and/or the bore had not separated from the cold front. This conclusion is supported by surface wind plots (Fig. 6) and streamline analysis (Fig. 3). It could also be that the bore was not separated enough from (or maybe even not triggered) the cold front.

At stations east of CART (OILT, BRIS, and to a lesser extent at OKMU), the bore was distinctly recognizable. It arrived at OILT, BRIS, and OKMU at 0700, 0720, and about 0810, respectively, and was associated with wind direction shifts, temperature increases, and pressure changes. Wind speed, however, decreased slightly at these stations contrary to that observed at the stations near the CART site. The magnitudes of the temperature increases were also smaller than stations near CART even though the pressure jumps were comparable (>2 mb). This suggests less vigorous mixing by the bore and/or an increase in the depth of the stable (nocturnal) boundary layer expected near sunrise. In general, this difference in the magnitude of the temperature increase is believed to be a function of the station temperature, the time of day (night), bore strength, inversion strength, and other local factors.

Using the above station datasets, a bore propagation speed of about 14 ± 0.5 m s^{-1} was calculated from a plot of the time of arrival of the pressure jumps at each

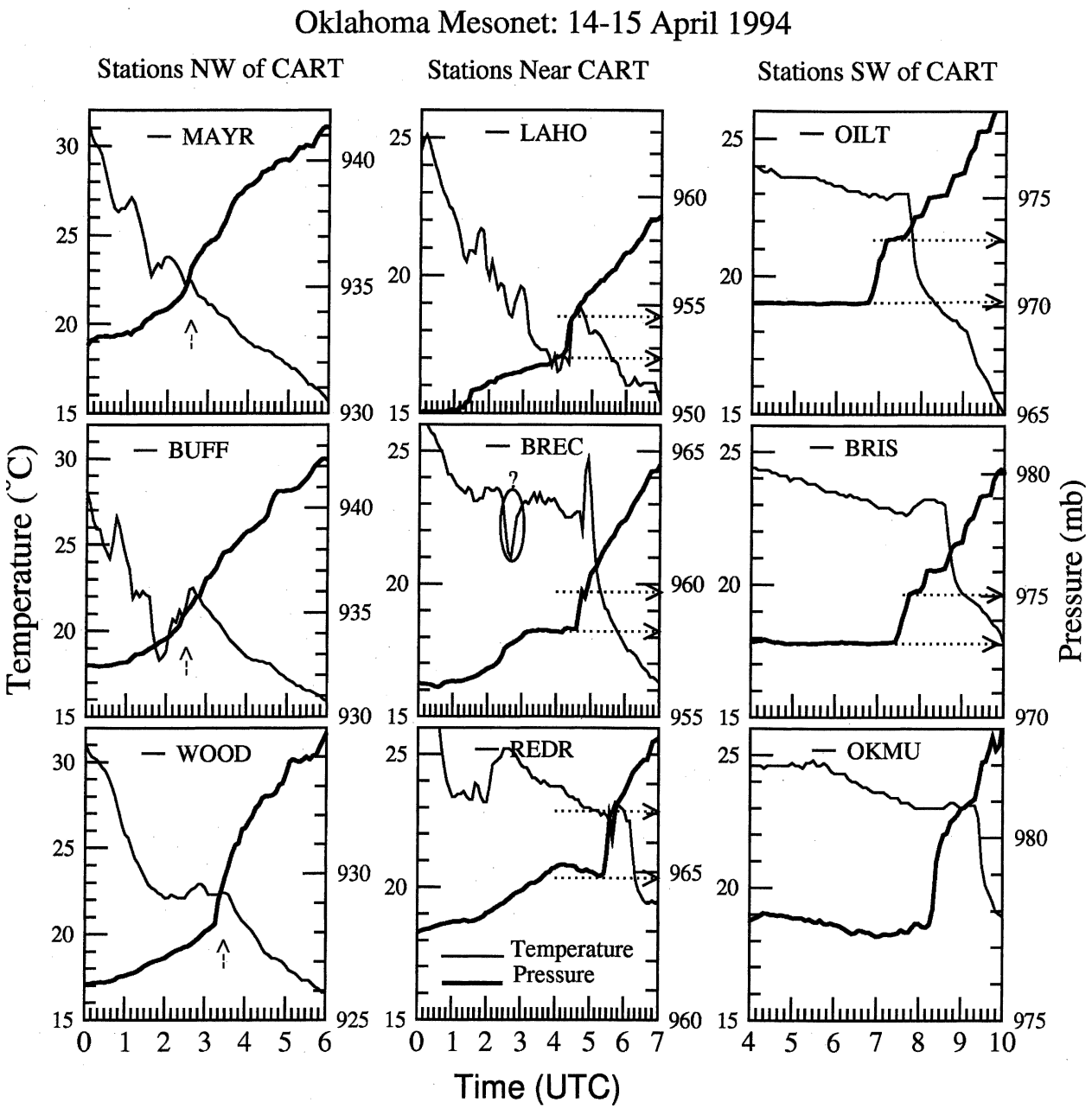

FIG. 5. Time series plots of temperature (°C) and pressure (mb) at selected stations, from the Oklahoma Mesonet, showing the pressure jump and its associated temperature perturbations on 14–15 Apr 1994.

station against the stations estimated distances from a reference point along a line that traverses the state from northwest to southeast (Fig. 7, dashed line). A similar propagation speed (14 m s^{-1}) was also calculated from the leading edge of the wind disturbance in Fig. 6; the trailing edge (surface cold-frontal passage for stations near CART) had a slower speed of about 11 m s^{-1}. A slightly higher bore propagation speed, 16 ± 0.6 m s^{-1}, was calculated from data taken at stations south of CART (Fig. 7, solid line).

d. Rawinsonde data

One of the mechanisms needed to sustain an atmospheric wave is a statically stable layer of air capped by a neutrally stable atmosphere. The vertical structure of the atmosphere on 14–15 April 1994 shows such stratification. Profiles of virtual potential temperature (θ_v), temperature, relative humidity, and wind speed and direction made at 0232 and 0545 on 14–15 April 1994 using radiosonde data at the CART site are plotted in

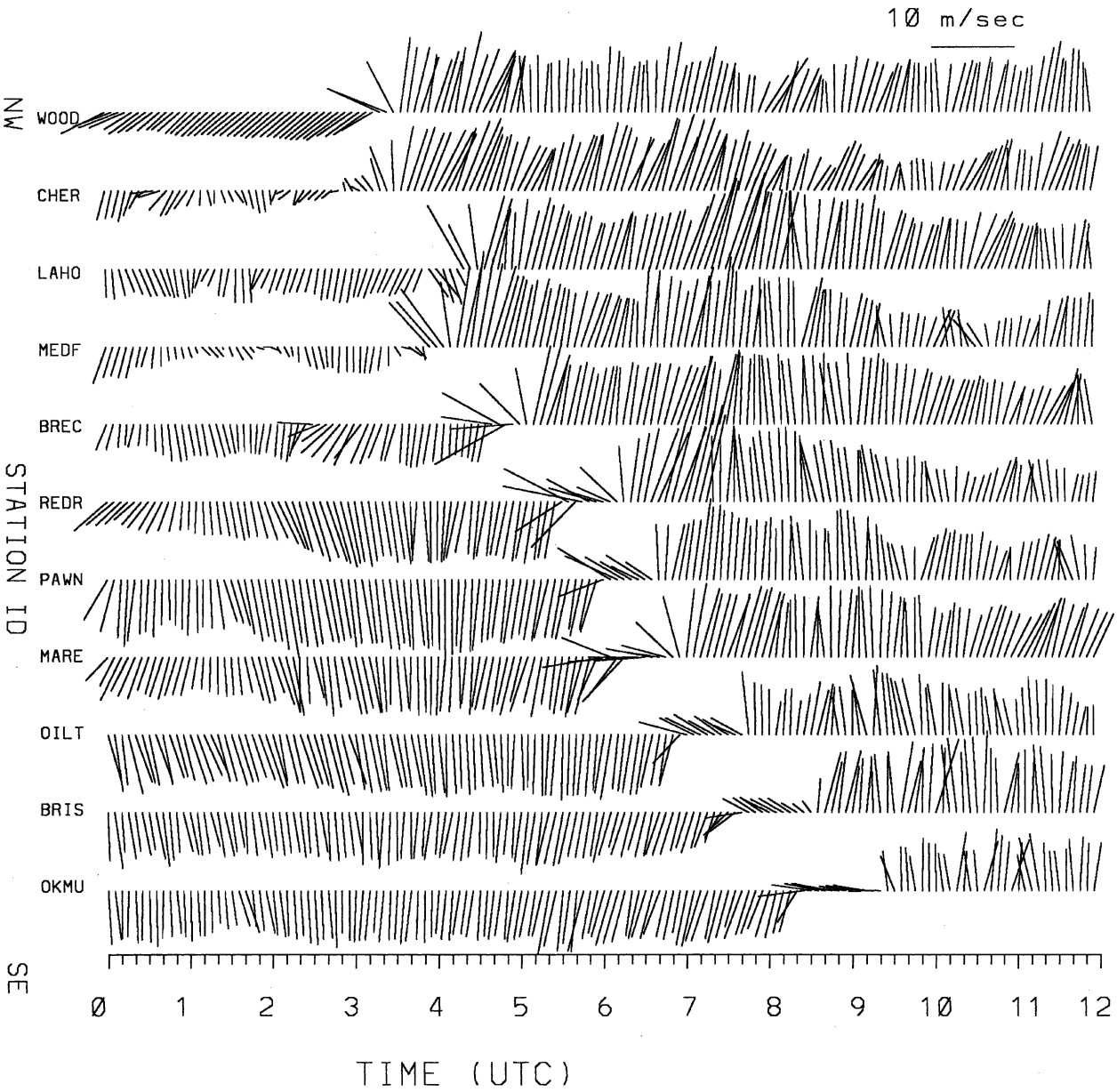

FIG. 6. Totem pole–type plot of time series wind vector data at selected stations from the Oklahoma Mesonet on 14–15 Apr 1994. The stations selected lie in a roughly NW–SE line across the state of Oklahoma. Note how the region of wind perturbation widens for stations in the SE.

Fig. 8. The θ_v sounding at 0232 was made when the dryline was located just west of the sampling area and will be used to study vertical structure evolution of the atmosphere during dryline conditions. The 0232 and the 0545 soundings represent prebore and postbore conditions, respectively.

In the 0232 sounding a stable layer near the ground extended to about 1 km, characterized by a $\Delta\theta_v$ of about 6° and Richardson number (Ri) of less than 1 indicating dynamic instability, and a Brunt–Väisälä frequency ($2\pi/N$) that increased linearly from 10 to about 25 min. This stable layer was topped by a second well-mixed layer (with a $\Delta\theta_v$ of about 2° between its top and base) extending to 5 km. Relative humidities were close to 20% at its base but progressively increased to about 90% near its top, which coincided with the passage of thin cirrus clouds. The Ri number at the base of this well-mixed layer (1.5–2.3 km) was significantly less than 0.25. A strong shear, exceeding 5 m s^{-1} km^{-1} throughout the lowest 2 km was also

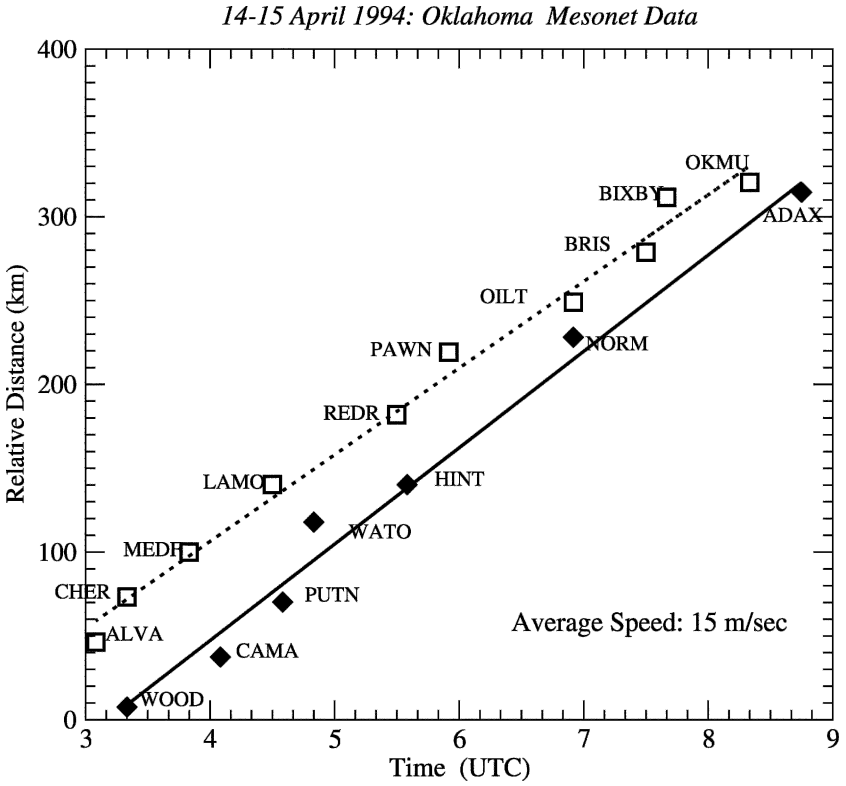

FIG. 7. Time of occurrence of the pressure jump, associated with the bore across stations along a line oriented in the direction of the bore movement (see inset figure) vs the relative distance from an arbitrary point in the NW corner of the state. A speed of propagation of the bore is calculated from the slope of the lines.

observed, suggesting favorable conditions for wave generation by wind shear as described by Gedzelman and Rilling (1978), Hauf (1993), and Hauf and Clark (1989).

The 0545 sounding revealed an atmosphere greatly modified by the cold-frontal system. It shows a cool, constant θ_v layer of about 500 m deep capped by a sharp inversion. The inversion at 0.7–1 km identifies the cold-frontal surface that lifted the moist air as the front moved eastward forming an elevated moist (RH $\cong$ 70%) layer. Between 1- and 2-km altitude, conditions were much colder than the same layer at 0232 and also of constant θ_v. Overlaying this lifted moist layer was the well-mixed midtropospheric layer identified on the 0232 sounding. The characteristics of this well-mixed layer stayed more or less the same as in the earlier soundings except that its depth was reduced by about 1 km as a result of the lifting of its base by the cold-frontal surface and slight lowering of its top. The amount of cooling at low levels in the 0545 sounding ranged from 10° at the lowest layer (0. to 0.5 km) to 11° between 0.5 and 1.75 km.

Also shown in Fig. 8 are wind speed and direction profiles that show the development of a jet at about 1 km with speeds of about 17–20 m s^{-1}. Above the low-level jet, wind speeds generally decreased to about 2 km before increasing again to more than 20 m s^{-1} near the top of the well-mixed layer. Near-surface wind directions were from the south-southwest but veered with height below 2 km and remained from the southwest during the 0232 sounding. Note that this wind direction profile supports the assertion made earlier that the air immediately west and above the dryline is similar. However, by 0545, while the direction above 2 km stayed the same as that of the earlier sounding, the low-level wind profile changed markedly; wind direction was northerly, a sign of the cold-frontal airmass dominance.

3. Raman lidar and radiometer measurements

a. Raman lidar measurements

Two Raman lidars, the National Aeronautics and Space Administration (NASA) Goddard Space Flight Center (GSFC) Scanning Raman lidar (SRL) and a sys-

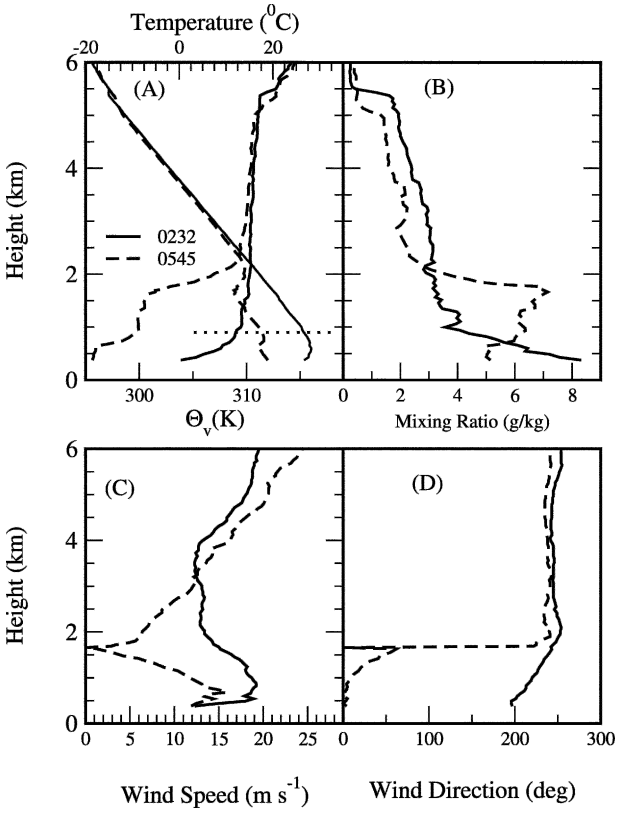

FIG. 8. Radiosonde-derived profiles of (a) θ_V, (b) temperature (°C) and relative humidity (%), (c) wind speed (m s^{-1}), and (d) wind direction (°) at 0232 and 0545 UTC 14–15 Apr 1994.

tem developed by Sandia laboratories prior to the operational ARM CART Raman lidar [referred to as the "Sandia lidar"; details can be found in Bisson et al. (1999) and Goldsmith et al. (1994)] were in operation during the ARM RCS IOP (Melfi et al. 1995, 1989; Starr et al. 1995). The measurement principle of both Raman lidars (RLs) is based on the theory that the ratio of the mass of the water vapor to that of the mass of dry air in a given volume (water vapor mixing ratio) is proportional to the ratio of the Raman scattering by water vapor in the atmosphere to that of nitrogen (Melfi 1972). During the ARM RCS IOP, the SRL was operated only at night (daytime capabilities have since been added) while the Sandia lidar was deployed to test the now successful narrowband, narrow-field-of-view approach for making daytime Raman lidar measurements. The lidars were calibrated using coincident radiosonde measurements to derive a single calibration constant relating the lidar data to the radiosonde-derived water vapor mixing ratio data. In normal operation, thousands of laser shots are incorporated into a single 1-min water vapor profile with range resolution of 75 m. A full description, discussion, and enhancements through the years of the lidars can be found in Whiteman (2003), Whiteman and Melfi (1999), Whiteman et al. (1992, 2001), Ferrare et al. (1995), Goldsmith et al. (1994), and Turner and Goldsmith (1999). Comparisons of the lidars' performance with other sensors have revealed high correlations in the past as reported by England et al. (1992), Soden and Bretherton (1994), Ferrare et al. (1995), and Wang et al. (1995). An example of a comparison of SRL and radiosonde-measured water vapor mixing ratios, as well as a plot of the SRL error analysis, is shown in Fig. 9.

Figure 10a reveals the state of the atmosphere over the CART Central Facility site as manifested by the high-vertical-resolution (75 m) water vapor mixing ratio profiles detected by the SRL from near surface to above 8 km on 15 April 1994, except for the data gap of about 10 min at about 0310 (when the SRL was down) and during heavy cloud occurrences where the laser beam gets attenuated rapidly (above 1 km at 0430 and above 4 km around 1000, when the data were limited to below cloud base). A higher temporal resolution, time–height evolution of the atmosphere is also shown in Fig. 10b using the data from the Sandia lidar. Note that the Sandia lidar was operating in a conventional, vertical-only, 1-min data acquisition mode while the SRL was operating in a "scanning" mode in which vertical-pointing data were acquired only every other minute, leading to some decrease in its effective temporal resolution especially in capturing the small-scale details of the bore undulations (Fig. 10a). Relative humidity values, derived using the data in Fig. 10 and radiosonde temperature profiles, are plotted in Fig. 11. The sudden moistening of the lower atmosphere (0.5–1.5 km) around 0300, the dramatic boundary layer undulations near 0430, and the change to a drier boundary layer capped by a slanted frontal surface was a result of the interplay between the moisture tongue moving north from the Gulf and the approaching cold front from the west as pointed out in the earlier sections and referred to as "frontal-dryline merger" in Parsons et al. (2000).

Figure 10 may be partitioned into three distinct time regions, for analysis purposes, based on the surface wind direction and the moisture structure.

1) TIME PERIOD I (PRIOR TO 0430)

This time period represents the arrival of the dryline over the sampling site. This moisture tongue over the site was a result of the westward advance of the dryline early during the night, consequent stagnation, and then later retreat. Much of the pre-dryline air was not sampled since the lidar operation on that night did not

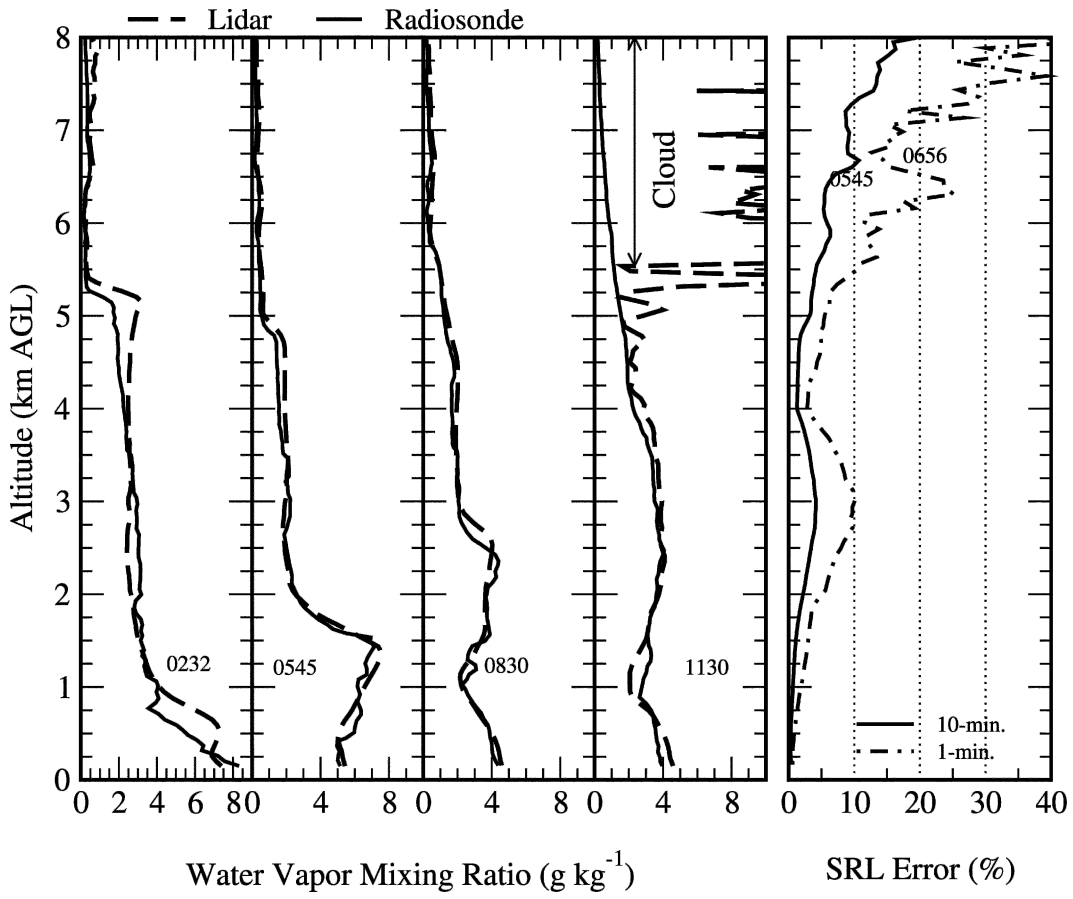

FIG. 9. Comparison of SRL- and radiosonde-measured water vapor mixing ratio (g kg^{-1}) profiles and SRL error analysis on 14–15 Apr 1994. SRL profiles were averaged to within ±15 min of the time of radiosonde launch.

start until 0240. However, by using the 9 g kg^{-1} isohume (Schaefer 1986), the vertical and horizontal (east–west) structure of the dryline is superbly visualized by the lidar data.

A number of dryline characteristics are revealed by the finescale Raman lidar data. The high moisture contrast between the air west of the dryline and the dry air above (believed to have similar characteristics) to the air mass east of the dryline is evident. The nearly vertical boundary between the moist and dry air to the west, a result of the nonexistent temperature discontinuity (Hess 1959, 232–234), is clearly evident. The slight tilt of the 9 g kg^{-1} isohume (Fig. 10a, the leading edge of the green region) eastward in the lidar data is in agreement with the findings of Fujita (1958) and McGuire (1962). The 9 g kg^{-1} isohume was preceded by a region of drier air mass (mixing ratio of about 5 g kg^{-1}) that was lifted and arched through 90° to form a horizontal lid on top of the moist air forming the dryline that extended to about 1.2 km above ground level. The 5 g kg^{-1} shading also separates the low-level moisture from the well-mixed (1–2 g kg^{-1}) layer that extends through the midtroposphere as shown from the radiosonde profiles presented earlier and also observed by Carlson and Ludlam (1968) and Schaefer (1986). This steplike structure of the boundary layer in the lower levels is also similar to the steplike structure found from radiosonde profiles reported by Schaefer (1986). A contour plot of equivalent potential temperature (θ_v), derived from a combination of the three soundings on this day (at 2332, 0232, and 0545) and the SRL-measured mixing ratio data (Fig. 12), also reveals this steplike atmospheric structure and the well-mixed layer aloft. Note the gradual decrease in the depth of the well-mixed layer from more than 3.5 km deep at about 0240 to about 1 km by 1100.

Considerable finescale perturbations were also observed along the moist–dry transition near the inversion layer. The RL data during this time were filled by waves, of about 5-min peak-to-peak distances, visible throughout the depth of the dryline. The most intense of these waves occurred around 0320 and coincided

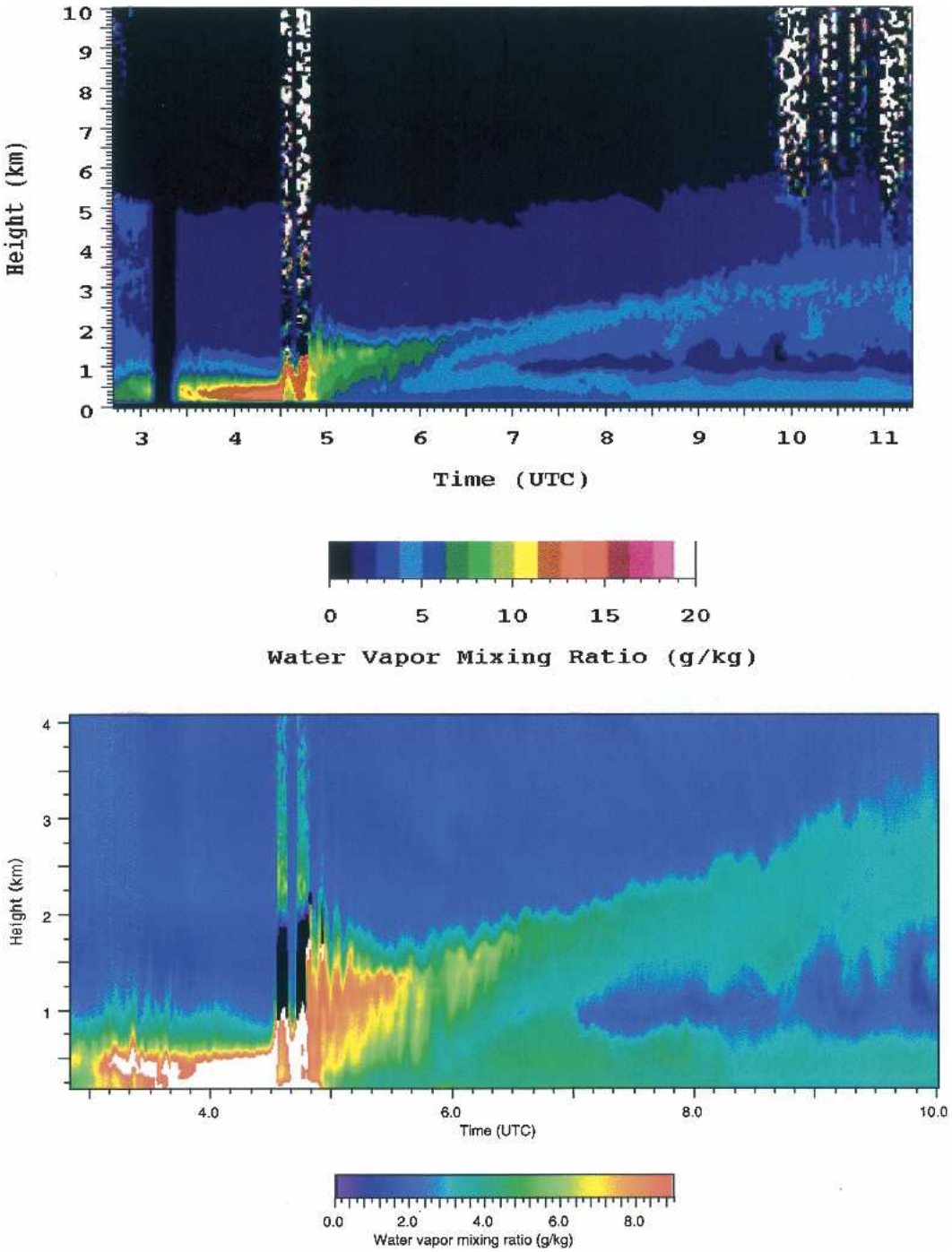

FIG. 10. Color-coded image of the water vapor mixing ratio (g kg^{-1}) profiles measured by the (top) SRL and (bottom) Sandia lidar on the night of 14–15 Apr 1994 over the CART station. Note the data gap around 0310 UTC in the top image and the vertical striping around 0430 UTC and near the end, which indicate laser beam attenuation by clouds. Note that the SRL was operated in "scan" mode and data shown here are vertical profiles only (made every other minute), while the Sandia lidar was operated in vertical-only, 1-min resolution.

with the temperature, wind speed, wind direction, and pressure perturbations discussed earlier. Between 0400 and 0430, the air on top of the dryline, between mixing ratio contour lines of about 9 and 5 g kg^{-1} (Fig. 10), shrunk in depth by about 0.25 km, reminiscent of a supercritical flow region (Turner 1979, p. 67) obstructed by the approaching cold front that led to the pressure jump at 0430.

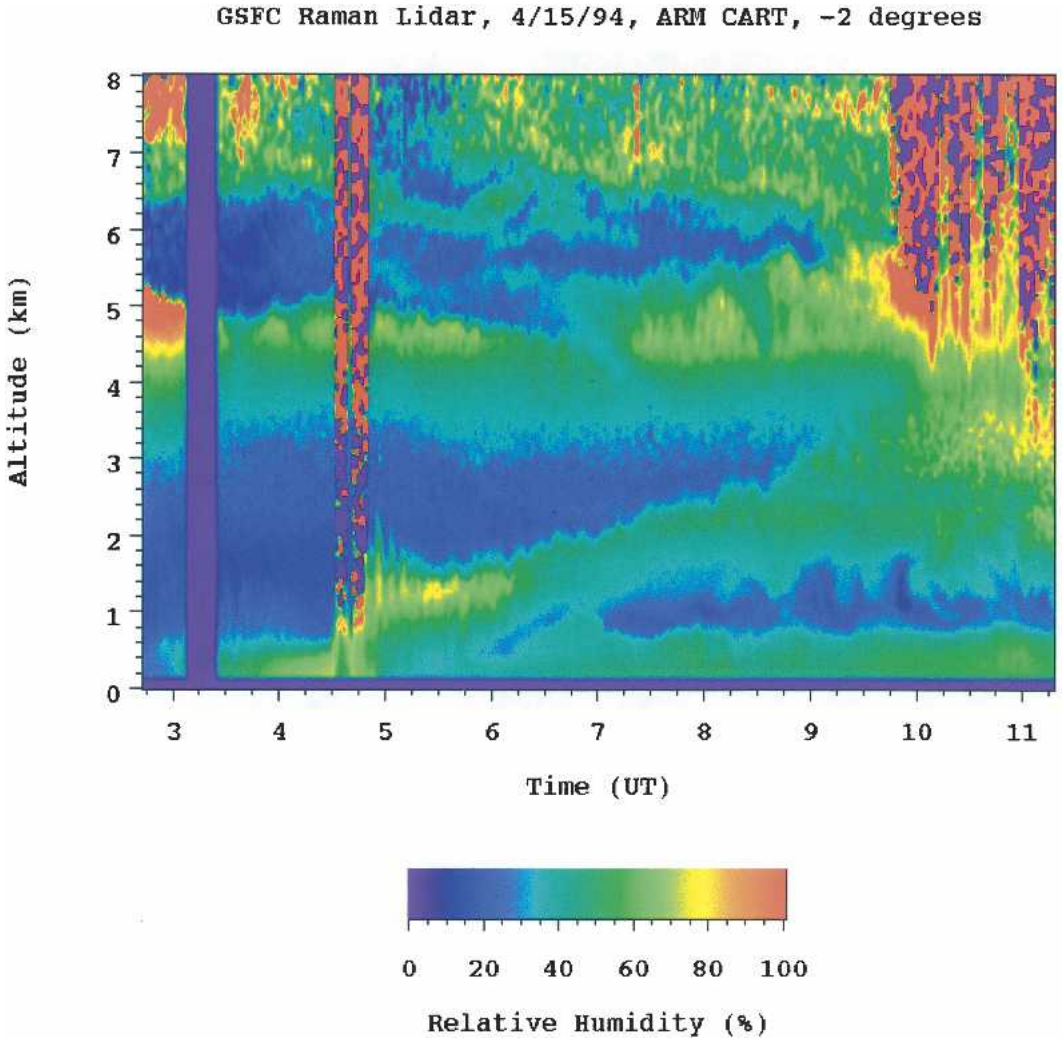

FIG. 11. Color-coded image of relative humidity (%) derived using the SRL water vapor mixing ratio profiles and rawinsonde temperatures on the night of 14–15 Apr 1994.

2) TIME PERIOD II (0430–0530)

The low-level moisture during this time was regulated mainly by the undular bore oscillations. The pressure jump at 0430 and the undulations that followed produced intense mixing in the low-level moisture field. Associated with this intense mixing and abrupt increase in height of the low-level moisture was a slight decrease in the depth of the well-mixed layer on top. It is important here to point out the advantage of a moisture-sensing profiler instrument like the RL over that of standard surface-based or radiosonde (3-h intervals at best) instruments in resolving these short, transient waves and associated atmospheric structure. The high resolution in time and height and the fact that no large temperature lapse rates or dust particles are required (as would be required by acoustic sounders and most radars, respectively) makes the RL a superior instrument in visualizing atmospheric moisture structure.

Recall from earlier discussions that the pressure jump at 0430 had a magnitude of about 1.9 mb in less than 2 min and led to the formation of low-level clouds. Since the SRL was not able to penetrate these dense clouds (high cloud liquid water content), as will be shown later, data from other sources (from the University of Utah lidar and Pennsylvania State University 94-GHz radar; not shown here) were used to estimate cloud-top altitude and geometric structure. The first cloud band (base 1.33, top 1.5 km) occurred between 0431 and 0439 and coincides well in time with the time of the large pressure jump recorded at the surface. The second cloud band also had a slant base that varied in altitude from about 1.33 km at 0441 to about 1.75 km at 0451 with a cloud-top height of 2.23 km. A third, thin

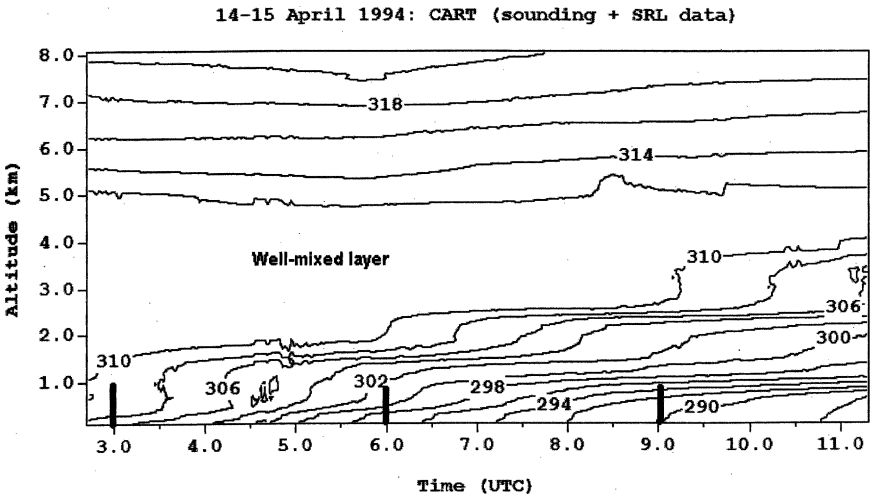

FIG. 12. Equivalent potential temperature (K) derived from a combination of three soundings (at 2332, 0232, and 0545 UTC) and the lidar mixing ratio data. Note the steplike vertical structure and the decreasing depth of the well-mixed layer between the 310- and 312-K contour lines. The heavy vertical lines indicate the approximate time of the soundings (shown in Fig. 8).

haze/cloud layer was also observed topping the third wave peak. The undulations continued with decreased amplitude, no cloud formation, and decreased period (peak-to-peak time). For example, the first two wave peaks were about 10 min apart while the separation between the third and fourth waves was shorter, at about 8 min. This was also true for the other wave peaks and may be linked to the shrinking depth of the low-level moist layer, a subject of a forthcoming article.

In addition to the bore undulations, measurements of the RL in this time period revealed all the layers identified in the rawinsonde profiles earlier as layers of contrasting moisture. These include the moist layer below about 2.0 km, the well-mixed midtropospheric layer, and the dry layer above 5 km. Note that the depth of the well-mixed layer progressively decreased not only because the top of the layer (mixing ratio of about 2.0 g kg^{-1}) decreased, but also because of the substantial lift due to the intense mixing associated with the bore and cold-frontal surface from below.

3) TIME PERIOD III (LATER THAN 0530)

This time period was characterized by the dominance of the cool and dry air mass behind the cold front. The sloping frontal surface, the undulations on the frontal surface and the mixing processes that resulted, the cloud formation about 5–6 h after the surface cold-frontal passage, and the decrease in depth and eventual demise of the midtropospheric layer are all visualized by the RL data and agree well with the results obtained from radiosonde, surface, and satellite observations.

Recall again that locating the exact time of the surface cold-frontal passage was complicated by the presence of the bore undulations. However, as can be seen in Fig. 10, this task is simplified by using the high temporal and vertical profiles of the RL. Assuming the 5 g kg^{-1} isohume separates the humid air mass from the south and the cold–dry air from the west, Fig. 10 indicates the frontal passage to be about 0530. Recall also that the lowest temperature recorded immediately following the bore undulations was at 0530. However, mixing ratio values greater than 5 g kg^{-1} were observed at low levels (surface to about 500 m) until about 0820, which suggests that the leading edge of the cold-frontal air mass was detached from the surface forming the frictional layer. Finally, the RL measurements also revealed that the cold-frontal surface was characterized by extensive undulations that later changed into broken cellular structures indicative of vigorous mixing processes; the downward mixing of parcels can be traced as 5 g kg^{-1} fingers digging deep down into the cold air mass.

b. Microwave radiometer

The column-integrated PWV and liquid water content (LWC) were simultaneously recorded during the ARM experiment using a microwave radiometer located at the CART Central Facility site (Liljegren and Lesht 1996). The existence of clouds and the effect of the undulations observed during the night on the integrated moisture of the entire atmospheric column can also be seen from the microwave-radiometer-measured

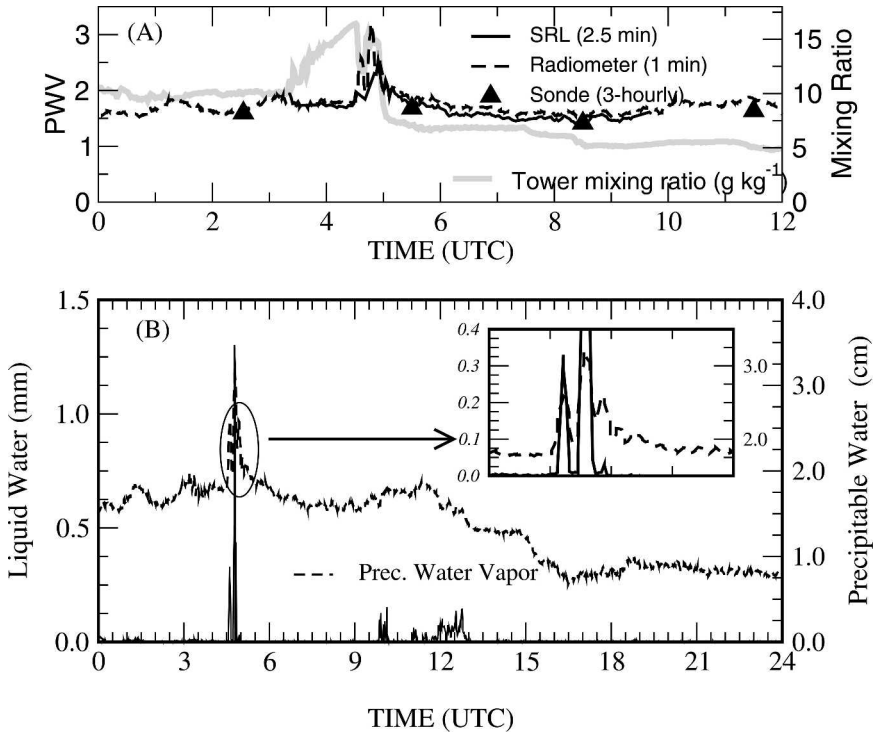

FIG. 13. (a) Comparison of nighttime SRL data with the radiometer- and radiosonde-measured precipitable water vapor on 14–15 Apr 1994. (b) Details of the radiometer-measured liquid water and precipitable water content during the undular bore on 15 Apr 1994.

PWV and LWC. In Fig. 13a, a comparison of PWV derived from the SRL, radiosonde, and the radiometer during the night of 15 April 1994 is presented. A very good agreement in the temporal trend between the datasets was found. Slightly larger magnitudes of radiometer PWV over that of the SRL were believed to be due to the fact that the SRL is "blind" to low-level moisture (below an elevation of 170 m) and the fact that it is calibrated using the sondes, which are drier than the radiometers (see Ferrare et al. 1995; Turner et al. 2003).

The dramatic boundary layer undulations that occurred during the night were also captured by the radiometer-measured PWV (Fig. 13b). At 0430, the PWV and LWC increased to unusually large amounts associated with the pressure jump and the accompanying undular bore oscillations. The oscillations consisted of two main cloud rolls of about 10 min long and a third peak of shorter duration and lower LWC (most likely a haze layer). Among the three waves that were recorded between 0430 and 0500, the second wave had the highest LWC and amplitude of oscillation, with both the others showing a modulated drop in amplitude. The envelope of these three wave peaks was approximately one period (about 2 h) away from the peak at 0320, suggesting that it could be an extension of the wave of period about 2 h that peaked at about 0120 and 0320. In addition, the PWV curve shows two distinct and long wave peaks centered at about 0120 and 0320 that coincided with the small temperature, pressure, and wind speed increases, as well as wind speed shifts at the site as discussed earlier. It is interesting to note that the amount of low-level moisture (tower data) continued to increase between 0320 and 0430 while radiometer-measured PWV stayed almost constant, an indication of subsidence (drying) aloft. Tower-measured mixing ratio (g kg^{-1}) data are also included to indicate the dryline position and for comparison purposes.

Smaller-amplitude (and period) waves in the radiometer-measured PWV values persisted throughout the night. For example, a set of oscillations (period of 5 min) between 0530 and 0600 followed by a drop and then more oscillations between 0800 and 1000 (30 min) were observed. A complete analysis of these waves using the wavelet analysis methods is the subject of a forthcoming paper.

4. Theoretical considerations

There are a number of numerical and theoretical studies of bores and related phenomena in the litera-

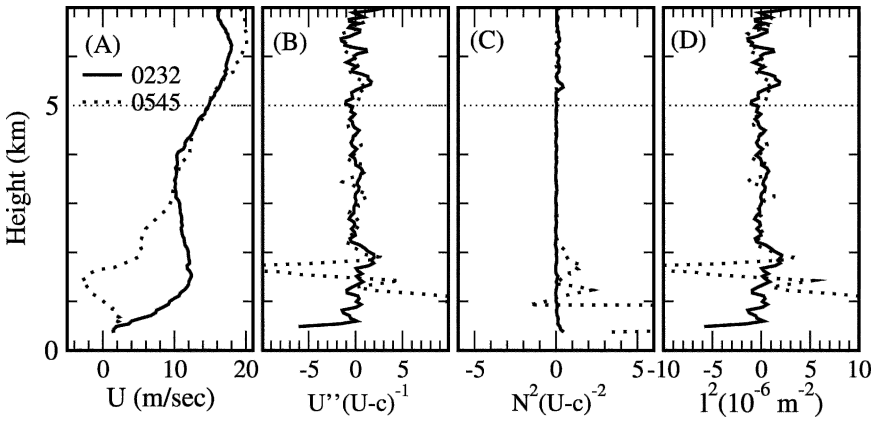

FIG. 14. Bore-ducting analysis based on the 0232 and 0545 UTC 15 Apr 1994 soundings. Shown are profiles of wind components in the direction of (a) bore propagation, (b) the curvature, and (c) the stability terms that contribute to the (d) Scorer parameter.

ture. These include the early work of Benjamin (1967), a review by Simpson (1987), and also the work of Christie et al.(1978) and Christie (1989), Crook (1984, 1988), Crook and Miller (1985), Smith (1988), Doviak et al. (1991), and references therein. Here, we attempt to compare the observation and theoretical predictions of some of the characteristics of the undular bore, but first we discuss the wave-ducting properties of the atmosphere.

A number of authors (Scorer 1949; Lindzen and Tung 1976; Crook 1988; and others) have suggested conditions for trapping the vertical leakage of wave energy in a stratified atmosphere. Solving a two-layer system analytically, Scorer (1949) explained that in order to have no vertical wave propagation, the vertical wavenumber must decrease with height to strongly negative values. The vertical wave parameter, m^2, is defined as

$$m^2 = \frac{N^2}{(U-c)^2} - \frac{U''}{U-c} - k^2, \qquad (1)$$

where $l^2 = m^2 + k^2 = (N^2/(U-c)^2) - (U''/U-c)$ is often called the Scorer parameter and is identical to the wavenumber in the case of long waves, $U - c$ is the ambient wind relative to the bore ground speed c, k is the horizontal wavenumber, N is the Brunt–Väisälä frequency within the stable layer, and $U''(z) = (d^2U/dz^2)$. The first and second terms in the right-hand side of Eq. (1) are also referred to as the stability and curvature terms, respectively. In the long-wave approximation, a decrease of l^2 with altitude from positive to negative values leads to the trapping of waves below a layer where $l^2 < 0$, leading to a ducting of waves in the horizontal for several periods.

In Fig. 14, the Scorer parameters for the soundings of 0232 and 0545 (i.e., about 2 h before and 1.5 h after the observation of the bore) are plotted. The profile of $U(z)$ was determined using 15 m s^{-1} and 280° for the bore speed and direction, respectively, as determined earlier. It exhibits a critical level around 5 km, and the effect of a developing low-level jet can be seen in the 0232 sounding around 1.5 km while the 0545 sounding at low levels was modified by the cold-frontal system. In addition, the 0232 sounding shows an increase of l^2 with altitude, which is not conducive for trapping vertical wave propagation. However, by 0545, the Scorer parameter, dominated by the stability term, decreased with height from positive to strongly negative values up to about 2-km altitude, near the top of the moist layer in Fig. 10. Thus, in conclusion, we believe that the approaching cold front from the west served as the triggering mechanism that lead to the observed flurry of wave activity. The low-level stable air, a vertical profile of the Scorer parameter that decreased to strongly negative values at the top of the moist stable layer, and a low-level jet opposing the wave motion all contributed to the wave-trapping mechanism ensuring the ducting of the waves generated (Crook 1986).

The speed of the bore on a continuously stratified fluid may be written as (Crook and Miller 1985), neglecting wind shear effects,

$$C_{\text{bore}} = \frac{2Nd}{\pi}, \qquad (2)$$

where d is the mean height of the bore. According to Crook and Miller (1985), the value of d in Eq. (2) is determined from the undulations "as far from the leading edge of the bore as possible where the wave amplitude is small." However, as can be seen from the RL measurements (Fig. 10), the sloping cold-frontal surface following the bore complicated exact determination of

this parameter. Regardless, the mean depth was estimated to be about 1.9 km (between the fourth and fifth wave peak, at about 2 km, and where the oscillations seem to start to fade, at about 1.7 km). Using the 0232 sounding, a mean N for the stable layer ($\Delta\theta_v = 6$ K in a 1-km layer) was calculated to be 1.37×10^{-2} s^{-1}. These values predict a bore speed of 14 m s^{-1}, which is in good agreement with the propagation speed of about 15 m s^{-1} found earlier from the mesonet observations.

Note that the speeds become essentially the same if the bore speed is calculated in the frame of reference in which the upstream air at low levels is essentially at rest (Fig. 14a, ~1 m s^{-1}).

The bore speed was also calculated using the two-layer fluid model of Rottman and Simpson (1989), which hydraulic theory predicts to be a function of the fluid interface depth (h_0), the bore depth (h_1), and inversion strength ($\Delta\theta$) as $C_{\text{bore}} = ((g\Delta\theta/\theta)h_0)[\frac{1}{2}(h_1/h_0)(1 + (h_1/h_0))]^{(1/2)}$.

Using $h_0 = 0.8$ km, $h_1 = 1.2$ km, and $\Delta\theta = 5$ K, this relationship yields a speed of about 16 m s^{-1}, again in fairly good agreement with the speed derived from mesonet data of Fig. 7.

5. Summary and conclusions

During the night of 14–15 April 1994, moist air moving northward from the Gulf of Mexico converged with a cold-frontal air mass from the northwest over north-central Oklahoma in the presence of a well-mixed midtropospheric layer. Surface mesonet records, rawinsonde soundings, the moisture-profile-sensing NASA GSFC scanning Raman lidar (SRL), the Sandia Raman lidar, and microwave radiometer revealed that the convergence of these two airmass systems led to the initiation and propagation of an undular bore. This paper discussed the evolution of the atmospheric structure during the night.

A greater emphasis was given to demonstrating the ability of Raman lidars (RLs) in visualizing the fine-scale features of the nocturnal boundary layer structure, which resulted from the interaction of these mesoscale processes, using the water vapor mixing ratio. A comparison of the RL measurements with rawinsonde and surface-based instruments showed that the RL accurately, and with very high resolution, described the moisture profiles that resulted during the dryline, the approaching cold front, the bore and associated undulations, as well as the upper-level moisture up to about 8-km altitude. In the RL profiles, the dryline was apparent as a moist steplike structure of height less than 1 km and lasted for about 2 h. The moist–dry boundary at about 1-km altitude was characterized by high frequency (≈10 min or less) during these 2 h before being swept out of the area by the cold front. This dryline–front interaction (or "merger") led to the undular bore that propagated in a southeasterly direction ahead of the cold front at a speed of about 15 m s^{-1}. The moisture structure, amplitude, duration and dissipation of the bore undulations, and the progressive decrease in wavelength of the bore undulations (12 min for the first wave to 7 min by the fifth wave, all in less than 30 min) were clearly identifiable from the SRL measurements.

The RL measurements also revealed a detailed structure of the boundary layer during the cold-frontal period. At the surface, the front arrived more than a half hour behind the undular bore, an observation difficult to obtain accurately from satellite and surface mesonet records for such cases. The complicated structure of the leading edge of the cold-frontal air mass and its interaction with the moist Gulf air riding the sloped frontal surface, the mixing of the moist air across the frontal surface, the location of clouds about 5 h behind the surface front, as well as the moisture structure within the cold-frontal air mass, were clearly detected and visualized. Note that during the dryline–front merger, although the warmer of the two flows was lifted over the cooler, denser boundary to more than 1-km altitude, no extensive clouds were observed. Only the roll clouds, topping the vigorous bore undulations, were observed.

Rawinsonde, surface mesonet, and microwave radiometer datasets confirmed the SRL observations. The dryline and subsequent moistening was detected by a tower- (60 m) mounted humidity sensor, and the temporal values correlate well with those of the RL data. A pressure rise (1.9 mb), temperature perturbation (a brief dip followed by a pronounced rise of about 3°C), and wind shifts, which were all associated with the undular bore, were recorded. A number of coinciding prebore perturbations were also observed in the surface and RL data. The thermodynamic profiles made before and after the bore passage revealed an atmospheric structure conducive to horizontal wave propagation, that is, a stable layer near the surface (acting as a duct for the waves generated) topped by a well-mixed midtropospheric layer that suppressed the vertical propagation of waves.

High-resolution microwave radiometer measurements of precipitable water vapor and column-integrated cloud liquid water values were also recorded during the night. A substantial amount of precipitable water vapor (3.4 cm during the second peak of the bore oscillation) and column-integrated cloud liquid water (1.3 mm) were generated by the convection initiated by the bore undulations. Very good agreement between

the radiometer and the RL measurements was also found.

Finally, this work has presented the utility of the RL for high-resolution study of the boundary layer structure. The RL data reported are the most detailed observations yet obtained of the atmospheric structure during the development of an undular bore that resulted from the interaction of a cold front and a stable moist layer associated with a dryline. The successful operation of the Sandia lidar has led to the operational U.S. Department of Energy (DOE) ARM Raman lidar at the CART site, which has amassed more than 6 yr of day/night continuous data. With its recent enhancements in daytime atmospheric sensing and possible future temperature and liquid water probing potential, the NASA GSFC SRL offers a great opportunity in mobile, high-resolution study of the boundary layer and mesoscale phenomena.

Acknowledgments. We wish to acknowledge the support of the Atmospheric Radiation Measurement Program for our participation in the 1994 Water Vapor IOP and Dr. Ramesh Kakar, head of NASA's Atmospheric Dynamics and Remote Sensing Program, which made this work possible. Data measured by the microwave radiometer, radiosonde, tower, and Oklahoma Mesonet data were provided by the U.S. Department of Energy as part of the Atmospheric Radiation Measurement Program. This research was also supported by National Science Foundation Grant ATM-0129605, made to Belay B. Demoz when he was at the University of Maryland, Baltimore County.

REFERENCES

Ackerman, T., and G. Stokes, 2003: The Atmospheric Radiation Measurement Program. *Phys. Today,* **56,** 38–45.

Benjamin, T. B., 1967: Internal waves of permanent form in fluids of great depth. *J. Fluid Mech.,* **29,** 559–592.

Bisson, S. E., J. E. M. Goldsmith, and M. G. Mitchell, 1999: Narrow-band, narrow-field-of-view Raman lidar with combined day and night capability for tropospheric water-vapor profile measurements. *Appl. Opt.,* **38,** 1841–1849.

Carlson, T. N., and F. H. Ludlam, 1968: Conditions for the occurrence of severe local storms. *Tellus,* **20,** 203–226.

Cheung, T. K., and C. G. Little, 1990: Meteorological tower, microbarograph array, and sodar observations of solitary waves in the nocturnal boundary layer. *J. Atmos. Sci.,* **47,** 2516–2536.

Christie, D. R., 1989: Long nonlinear waves in the lower atmosphere. *J. Atmos. Sci.,* **46,** 1462–1491.

——, K. J. Muirhead, and A. L. Hales, 1978: On solitary waves in the atmosphere. *J. Atmos. Sci.,* **35,** 805–825.

Clarke, R. H., 1983: The morning glory. *Weatherwise,* **36,** 134–137.

——, R. K. Smith, and D. G. Reid, 1981: The morning glory of the Gulf of Carpentaria: An atmospheric undular bore. *Mon. Wea. Rev.,* **109,** 1726–1750.

Crook, N. A., 1984: The formation of the Morning Glory. *Mesoscale Meteorology—Theories, Observations and Models*, D. K. Lilly and T. Gal-Chen, Eds., Kluwer Academic, 349–353.

——, 1986: The effect of ambient stratification and moisture on the motion of atmospheric undular bores. *J. Atmos. Sci.,* **43,** 171–181.

——, 1988: Trapping of low-level internal gravity waves. *J. Atmos. Sci.,* **45,** 1533–1541.

——, and M. J. Miller, 1985: A numerical and analytical study of atmospheric undular bores. *Quart. J. Roy. Meteor. Soc.,* **111,** 225–242.

Doviak, R. J., and R. Ge, 1984: An atmospheric solitary gust observed with a Doppler radar, a tall tower and surface network. *J. Atmos. Sci.,* **41,** 2559–2573.

——, K. W. Thomas, and D. R. Christie, 1989: The wavefront, shape, position, and evolution of a great solitary wave of translation. *IEEE Trans. Geophys. Remote Sens.,* **27,** 658–665.

——, S. S. Chen, and D. R. Christie, 1991: A thunderstorm generated solitary wave observation compared with theory for nonlinear waves in a sheared atmosphere. *J. Atmos. Sci.,* **48,** 87–111.

England, M. N., R. A. Ferrare, S. H. Melfi, and D. N. Whiteman, 1992: Atmospheric water vapor measurements: Comparison of microwave radiometry and lidar. *J. Geophys. Res.,* **97,** 899–916.

Ferrare, R. A., S. H. Melfi, D. N. Whiteman, K. D. Evans, F. J. Schmidlin, and D. O. Starr, 1995: A comparison of water vapor measurements made by Raman lidar and radiosondes. *J. Atmos. Oceanic Technol.,* **12,** 1177–1195.

Fujita, T. T., 1958: Structure and movement of a dry front. *Bull. Amer. Meteor. Soc.,* **39,** 574–582.

Fulton, R., D. S. Zrnic, and R. J. Doviak, 1990: Initiation of a solitary wave family in the demise of a nocturnal thunderstorm density current. *J. Atmos. Sci.,* **47,** 319–337.

Gedzelman, S. D., and R. A. Rilling, 1978: Short-period atmospheric gravity waves: A study of their dynamic and synoptic features. *Mon. Wea. Rev.,* **106,** 196–210.

Goldsmith, J. E. M., S. E. Bisson, R. A. Ferrare, K. D. Evans, D. N. Whiteman, and S. H. Melfi, 1994: Raman lidar profiling of atmospheric water vapor: Simultaneous measurements with two collocated systems. *Bull. Amer. Meteor. Soc.,* **75,** 975–982.

Haase, S. P., and R. K. Smith, 1984: Morning glory wave clouds in Oklahoma: A case study. *Mon. Wea. Rev.,* **112,** 2078–2089.

——, and ——, 1989: The numerical simulation of atmospheric gravity currents. Part II: Environments with stable layers. *Geophys. Astrophys. Fluid Dyn.,* **46,** 35–51.

Hauf, T., 1993: Aircraft observation of convection waves over southern Germany—A case study. *Mon. Wea. Rev.,* **121,** 3282–3289.

——, and T. L. Clark, 1989: Three-dimensional numerical experiments on convectively forced internal gravity waves. *Quart. J. Roy. Meteor. Soc.,* **115,** 309–333.

Hess, S. L., 1959: *Introduction to Theoretical Meteorology*. Holt, 362 pp.

Koch, S. E., and W. L. Clark, 1999: A nonclassical cold front observed during COPTS-91: Frontal structure and the process of severe storm initiation. *J. Atmos. Sci.,* **56,** 2862–2890.

——, P. B. Dorian, R. Ferrare, S. H. Melfi, W. C. Skillman, and D. Whiteman, 1991: Structure of an internal bore and dissipating

gravity current as revealed by Raman lidar. *Mon. Wea. Rev.,* **119,** 857–887.

Liljegren, J. C., and B. M. Lesht, 1996: Measurements of integrated water vapor and cloud liquid water from microwave radiometers at the DOE ARM cloud and radiation testbed in the U.S. southern Great Plains. *Proc. Int. Geoscience and Remote Sensing Symp. (IGARSS),* Lincoln, NB, Geoscience and Remote Sensing Society, 1675–1677.

Lindzen, R. S., and K.-K. Tung, 1976: Banded convective activity and ducted gravity waves. *Mon. Wea. Rev.,* **104,** 1602–1617.

Locatelli, J. D., M. T. Stoelinga, P. V. Hobbs, and J. Johnson, 1998: Structure and evolution of an undulare bore on the high plains and its effects on migrating birds. *Bull. Amer. Meteor. Soc.,* **79,** 1043–1060.

Maxworthy, T., 1980: On the formation of nonlinear internal waves from the gravitational collapse of mixed regions in two and three dimensions. *J. Fluid Mech.,* **96,** 47–64.

McGuire, E. L., 1962: The vertical structure of three drylines as revealed by aircraft traverses. U.S. Weather Bureau, National Severe Storms Project Rep. 7, Kansas City, MO, 11 pp.

Melfi, S. H., 1972: Remote measurement of the atmosphere using Raman scattering. *Appl. Opt.,* **11,** 1605–1610.

——, D. N. Whiteman, and R. Ferrare, 1989: Observation of atmospheric fronts using Raman lidar moisture measurements. *J. Appl. Meteor.,* **28,** 789–806.

——, D. O'C. Starr, D. Whiteman, R. Ellingson, R. A. Ferrare, and K. Evans, 1995: Raman lidar measurements of water vapor and aerosol during the ARM RCS IOP. *Proc. ARM Science Team Meeting,* San Diego, CA, Dept. of Energy, 103–107.

Noonan, J. A., and R. K. Smith, 1986: Sea-breeze circulations over Cape York Peninsula and the generation of Gulf of Carpentaria cloud line disturbances. *J. Atmos. Sci.,* **43,** 1679–1693.

Parsons, D. B., M. A. Shapiro, and E. R. Miller, 2000: The mesoscale structure of a nocturnal dryline and of a frontal-dryline merger. *Mon. Wea. Rev.,* **128,** 3824–3838.

Peterson, R. E., 1983: The west Texas dryline: Occurrence and behavior. Preprints, *13th Conf. on Severe Local Storms*, Tulsa, OK, Amer. Meteor. Soc., J9–J11.

Ramamurthy, M. K., B. P. Collins, R. M. Rauber, and P. C. Kennedy, 1990: Evidence of very large-amplitude solitary waves in the atmosphere. *Nature,* **348,** 314–317.

Rottman, J. W., and J. E. Simpson, 1989: The formation of internal bores in the atmosphere: A laboratory model. *Quart. J. Roy. Meteor. Soc.,* **115,** 941–963.

Schaefer, J. T., 1986: The dryline. *Mesoscale Meteorology and Forecasting*, P. S. Ray, Ed., Amer. Meteor. Soc., 549–572.

Scorer, R. S., 1949: Theory of waves in the lee of mountains. *Quart. J. Roy. Meteor. Soc.,* **75,** 41–56.

Shapiro, M. A., T. Hampel, D. Rotzoll, and F. Mosher, 1985: The frontal hydraulic head: A meso-α scale ($\approx$1 km) triggering mechanism for mesoconvective weather systems. *Mon. Wea. Rev.,* **113,** 1166–1183.

Shreffler, J. H., and F. S. Binkowski, 1981: Observations of pressure jump lines in the Midwest. *Mon. Wea. Rev.,* **109,** 1713–1725.

Simpson, J. E., 1987: *Gravity Currents*. John Wiley & Sons, 244 pp.

Smith, R. K., 1988: Travelling waves and bores in the lower atmosphere: The "Morning Glory" and related phenomena. *Earth-Sci. Rev.,* **25,** 267–290.

——, N. Crook, and G. Roff, 1982: The morning glory: An extraordinary atmospheric undular bore. *Quart. J. Roy. Meteor. Soc.,* **108,** 937–956.

Soden, B. J., and F. P. Bretherton, 1994: Evaluation of water vapor distribution in general circulation models using satellite observations. *J. Geophys. Res.,* **99,** 1187–1210.

Starr, O'C. D., and Coauthors, 1995: Observation of a cold front with strong vertical undulations during the ARM RCS IOP. *Proc. 1995 ARM Science Team Meeting*, San Diego, CA, Dept. of Energy, 311–315.

Stokes, G. M., and S. E. Schwartz, 1994: The Atmospheric Radiation Measurement (ARM) Program: Programmatic background and design of the cloud and radiation test bed. *Bull. Amer. Meteor. Soc.,* **75,** 1201–1221.

Stull, R. B., 1988: *An Introduction to Boundary Layer Meteorology*. Kluwer Acadamic, 666 pp.

Tepper, M., 1950: A proposed mechanism of squall lines: The pressure jump line. *J. Meteor.,* **7,** 21–29.

Turner, D. D., and J. E. M. Goldsmith, 1999: Twenty-four-hour Raman lidar water vapor measurements during the Atmospheric Radiation Measurement Program's 1996 and 1997 water vapor intensive observation periods. *J. Atmos. Oceanic Technol.,* **16,** 1062–1076.

——, B. M. Lesht, S. A. Clough, J. C. Liljegren, H. E. Revercomb, and D. C. Tobin, 2003: Dry bias and variability in Vaisala radiosondes: The ARM experience. *J. Atmos. Oceanic Technol.,* **20,** 117–132.

Turner, J. S., 1979: *Buoyancy Effects in Fluids*. Cambridge University Press, 368 pp.

Wakimoto, R. M., and D. E. Kingsmill, 1995: Structure of an atmospheric undular bore generated from colliding boundaries during CaPE. *Mon. Wea. Rev.,* **123,** 1374–1393.

Wang, J. R., S. H. Melfi, P. Racette, D. N. Whiteman, L. A. Chang, R. A. Ferrare, K. D. Evans, and F. J. Schmidlin, 1995: Simultaneous measurements of atmospheric water vapor with MIR, Raman lidar, and rawinsondes. *J. Appl. Meteor.,* **34,** 1595–1607.

Whiteman, D. N., 2003: Examination of the traditional Raman lidar technique. II. Evaluating the ratios for water vapor and aerosols. *Appl. Opt.,* **42,** 2593–2608.

——, and S. H. Melfi, 1999: Cloud liquid water, mean droplet radius and number density measurements using a Raman lidar. *J. Geophys. Res.,* **104,** 31 411–31 419.

——, ——, and R. A. Ferrare, 1992: Raman lidar system for the measurement of water vapor and aerosols in the earth's atmosphere. *Appl. Opt.,* **31,** 3068–3082.

——, and Coauthors, 2001: Raman lidar measurements of water vapor and cirrus clouds during the passage of Hurricane Bonnie. *J. Geophys. Res.,* **106,** 5211–5225.